Intrinsic blinking characteristics of single colloidal CdSe-CdS/ZnS core-multishell quantum dots

Ying Fu*
Department of Applied Physics, Royal Institute of Technology, Science for Life Laboratory, SE-171 21 Solna, Sweden

Johnny Jussi
Department of Applied Physics, Royal Institute of Technology, Science for Life Laboratory, SE-171 21 Solna, Sweden and RISE Research Institute of Sweden AB, Box 1070, SE-164 25 Kista, Sweden

Louise Elmlund
Swedish National Forensic Centre, SE-581 94 Linköping, Sweden

Simon Dunne
Swedish National Forensic Centre, SE-581 94 Linköping, Sweden

Qin Wang
RISE Research Institute of Sweden AB, Box 1070, SE-164 25 Kista, Sweden

Hjalmar Brismar
Department of Applied Physics, Royal Institute of Technology, Science for Life Laboratory, SE-171 21 Solna, Sweden

(Received 6 September 2018; revised manuscript received 26 October 2018; published 2 January 2019)

Fluorescence blinking of single colloidal semiconductor quantum dots (QDs) has been extensively studied, and several sophisticated models have been proposed. In this work, we derive Heisenberg equations of motion to carefully study principal transition processes, i.e., photoexcitation, energy relaxation, impact ionization and Auger recombination, radiative and nonradiative recombinations, and tunneling between core states and surface states, of the electron-hole pair in single CdSe-CdS/ZnS core-multishell QDs and show that the on-state probability density distribution of the QD fluorescence obeys the random telegraph signal theory because of the random radiative recombination of the photoexcited electron-hole pair in the QD core, while the off-state probability density distribution obeys the inverse power law distribution due to the series of random walks of the photoexcited electron in the two-dimensional surface-state network after the electron tunnels from the QD core to the QD surface. These two different blinking characteristics of the single QD are resolved experimentally by properly adjusting the optical excitation power and the bin time.

DOI: 10.1103/PhysRevB.99.035404

I. INTRODUCTION

Quantum dots (QDs) are currently under close research and have been developed and used for many applications in many fields, including optoelectronics, biology, and medicine. QDs, especially colloidal semiconductor QDs, possess peculiar intrinsic fluorescence properties such as high quantum yields, narrow fluorescent spectra, broad absorption and excitation spectra with very little photobleaching. These characteristics make QDs an extremely powerful means for improving the efficiency of optoelectronics devices [1–4] and a versatile tool for both *in vitro* and *in vivo* biomedical applications such as single-particle tracking-and-delivery, nanotechnology-based carrier systems for traceable drug delivery and forensic genomic DNA quantification [5–9], as well as nondestructive industrial water-bath magnetic particle inspection assays [10].

Although many QDs have already been commercialized, intense fundamental research about them is still ongoing. One aspect in focus is the long-term nanotoxicity of QDs [11–14]. Another is the underlying physical mechanisms of a single QD's fluorescence blinking; that is, a single QD switches irregularly between bright (on) and dark (off) periods ranging from a millisecond to hundreds of seconds under continuous irradiation (see, e.g. Ref. [15–25]). It was found that the on- and off-state probability density distributions follow different rules. The off-state probability density distribution $P_{\rm off}(t)$ complies largely with the inverse power law; that is, $\log_{10}[P_{\rm off}(t)]$ is mostly linear in $\log_{10}(t)$, while in log-log scale the on-state probability density distribution $P_{\rm on}(t)$ bends upwards in the short time periods and falls off in the long time periods. Several qualitative and quantitative theoretical models have been proposed.

In the random telegraph signal model [15], the off periods are the times when the QD is ionized and the luminescence is quenched by nonradiative Auger recombination. A

*fu@kth.se

random Lévy-walk process was applied to study the long-period $P_{on}(t)$ and $P_{off}(t)$ [26,27]. The resultant $\log_{10}[P_{off}(t)]$ and $\log_{10}[P_{on}(t)]$ are both linear in t.

In biexciton and Auger ionization models [20], the probability of multiphotons per laser pulse that generated multiple excitons in a QD was studied and attributed to the falloff of $\log_{10}[P_{on}(t)]$ in the long time periods. However, why the multiphoton-multiexciton did not affect $P_{off}(t)$ was not discussed.

In the diffusion-controlled transfer model [28], a distribution of diffusion correlation times between the on state and the off state is proposed to model the different behaviors of the probability densities (one power characteristics in time duration from 100 os to 100 μs, and another different power characteristics in time duration from 100 μs to 100 s), though the separate behaviors in $P_{on}(t)$ and $P_{off}(t)$ were not studied.

In the multiple-recombination-center model [29], the recombination center (RC) has an active conformation and an inactive conformation. The QD off state corresponds to the active RC conformation such that the photogenerated hole becomes trapped by the active RC, then nonradiatively recombines with the photogenerated electron. When the RC assumes the inactive conformation, hole trapping is not efficient, and the QD stays in the on state.

In the hierarchical sequence model of the hole and electron trapping [30], the non-power-law behavior of $P_{on}(t)$ was attributed to a superposition of the hierarchical switching sequence of the hole and electron trapping involved in the surface structures of the QD.

The charge-tunneling and self-trapping (CTST) model assumes five principal states for the photogenerated electron and hole in the core and the surface of the CdZe-ZnS core-shell QD [31]. The tunneling of the carrier between the surface trap state and the core state is modeled by forward- and backward-tunneling barriers. Due to the differences in the forward- and backward-tunneling barriers, the simulated $P_{on}(t)$ clearly showed a falloff in long time periods, while $P_{off}(t)$ followed the power law in the time duration range from approximately 10^{-1} to $10^{1.5}$ s.

One major difficulty in understanding $P_{on}(t)$ and $P_{off}(t)$ is the lack of a quantitative match between theoretical simulations and experimental data in the time duration range from milliseconds to 100 s. Many proposed microscopic processes occur in the nanosecond even down to the picosecond scale, while a QD blinks at millisecond-second time duration. The CTST model showed quantitative agreement with experimental data in the time duration range of 10^{-1}–$10^{1.5}$ s, demonstrating the success of the model [31]. Compared with the CTST model, the charge-tunneling and surface-walking (CTSW) model recently published showed quantitative agreement in the whole time duration range of 10^{-3}–10^{2} s, which is the most common range for studying QD fluorescence blinking in the literature [32]. In this CTSW model, the off-state probability density distribution $P_{off}(t)$ of a single CdSe-CdS/ZnS core-multishell QD obeys the inverse power law distribution; that is, $\log_{10}[P_{off}(t)]$ displays a linear relationship to $\log_{10}(t)$ due to photoexcited electron tunneling out from the QD core performing a series of random walks in the two-dimensional surface-state network on the QD surface, while the on-state probability density distribution $\log_{10}[P_{on}(t)]$ displays a closer linearity with t because of the random radiative recombination of the photoexcited electron-hole pair in the QD core.

Although published experimental $\log_{10}[P_{off}(t)]$ data are mostly linear in $\log_{10}(t)$, reported relationships between $\log_{10}[P_{on}(t)]$ and t or $\log_{10}(t)$ vary greatly in terms of the QD structure, surface passivation, and/or modifications by various means [15,17,22,25,31]. The aforementioned CTSW model was derived from a number of series of CdSe-CdS/ZnS core-multishell QD structures and surface modification experiments [32].

Furthermore, a great variation can be observed in measurement setups. One key parameter is the excitation power that has been reported to greatly affect the QD blinking data which was attributed to multiphoton-multiexciton and other microscopic processes at high excitations [20,23]. Bin time used to measure QD blinking is the other key parameter that has also been shown to affect the apparent characteristics of $P_{on}(t)$ and $P_{off}(t)$ [24,29,33].

Thus, a mindful and thorough assessment of the relationships between the measurement setup, microscopic physical processes, and intrinsic blinking characteristics is greatly needed. In this work, we focus on the two key experimental parameters, namely, the excitation power and the bin time, in order to resolve the intrinsic QD fluorescence signal. Theoretically, the Heisenberg equations of motion of the electron-hole pair were explicitly derived for the CTSW model which was then further developed to include nonradiative energy relaxation processes. The model was applied to analyze our experimental data in order to resolve the intrinsic blinking characteristics of single QDs. It was further applied to discuss major experimental data about fluorescence blinking of different QDs in the literature.

II. EXPERIMENTAL RESULTS

A. QDs and blinking measurements

As briefly mentioned, apparent features of $P_{on}(t)$ and $P_{off}(t)$ vary greatly as functions of QD structure, surface modifications, and measurement setup. We focused on octadecylamine (ODA)-coated (oil-soluble) and 3-mercaptopropionic acids (3MPA)-coated (water-soluble) CdSe-CdS/ZnS core-multishell QDs. The 3MPA QDs were converted from ODA QDs; that is, their semiconductor structures were identical, and only surface ligands differed. These QDs were chemically synthesized in house and carefully characterized before [34,35].

QD samples for the fluorescence blinking study were prepared by depositing 5-μL QD solutions (concentration of 1 pM) on glass coverslips. After drying, the samples were mounted on an Axio Observer D1 microscope (Carl Zeiss) equipped with a mercury lamp (HBO 100, Carl Zeiss), a filter set (exciter: FF02-435/40-25, dichroic: FF510-Di02-25 × 36, emitter: FF01-500/LP-25, Semrock), an Electron-multiplying CCD (EMCCD) camera (Andor, 16 bit), and either a 100 × /1.4 oil immersion objective (Carl Zeiss), or a 64 × /1.4 oil immersion objective (Carl Zeiss). In our fluorescence imaging setup, QDs were excited by light within the wavelength range $\in$ (415, 455) nm centered at 436 nm from a mercury lamp. By adjusting the aperture diaphragm in the microscope and the

mercury lamp control panel, the excitation light power could be tuned. Five different excitation powers were used to excite QDs, which were calibrated by using an optical power meter (Thorlabs) to be 1.8, 3.9, 7.4, 12.1, and 25.0 W/cm^2.

The time series of the QD fluorescence emission were obtained by integrating the measured fluorescence intensity over time bins with a fixed interval, which is denoted as the bin time. During experiments with different excitation powers, the bin time of each image frame, 64×64 pixels ($6.4 \times 6.4\ \mu m^2$), was fixed to be 5.2 ms (exposure time of 4.29 ms and readout time of 0.91 ms). In our previous work we reported the measurement data of series consisting of 10 000, 50 000 and 100 000 frames where we did not observe any on and off events which lasted longer than 6000 frames [32]. Therefore, here we focus on time series consisting of 10 000 frames.

We further performed experiments with different bin times of each image frame of 20×20 pixels, from 2.8, 3.5, 6.2, and 8.9 up to 11.5 ms, with the excitation power fixed to 7.4 W/cm^2.

Note that the blinking measurement experiments were carried out on different days on QDs from different growth batches. We also analyzed the experimental data of CdSe-CdS/CdZnS/ZnS QDs and CdSe-CdS/ZnS QDs published previously [23]. The results presented below remain the same.

B. Single-QD blinking

One commonly increases the excitation power for a strong fluorescence signal assuming a linear relationship between the excitation power and fluorescence intensity; that is, the high excitation power does not induce extra physical processes. Typical fluorescence time series $I(t)$ of one single 3MPA QD are shown in Figs. 1(a)–1(d) under four different optical excitations. Two fluorescence states, the on state and off state, were easily identified from the occurrence profiles in Figs. 1(a′)–1(d′). It is observed here that at low excitations (1.8 and 3.9 W/cm^2) the fluorescence time series demonstrated clearly the on and off states, i.e., blinking. During the on states, $I(t)$ remained quite high above the background level, and during the off state, $I(t)$ remained closely at the background noise level. At too high excitation powers (12.1 and 25.0 W/cm^2) the peak of the on state in the occurrence profile became very broad, practically referred to as flickering. Excitation power thus could modify the characteristic appearance of the QD fluorescence blinking.

To show that the optical excitation power was well controlled, the background noise signal was checked and is presented in Figs. 1(a)–(d) as red lines. The excitation power was increased from 1.8 to 25 W/cm^2 by a factor of 13.9, while the average background noise signal increased only by a factor of 2 [see also the inset in Fig. 2(b)], most likely due to the less-than-perfect performance of the optical filters plus the scattered QD fluorescence lights.

We analyzed 150 ODA QDs and 120 3MPA QDs and found that the occurrence profile remained largely unchanged when the excitation power increased from 1.8 to 3.9 to 12.1 W/cm^2. The on-state peak in the occurrence profile became broad when the excitation power was further increased to 25 W/cm^2. Moreover, for many QDs with broad on-state occurrence peaks already at low excitations, the on-state occurrence peaks disappeared totally at high excitations; that is, they flickered at high excitations.

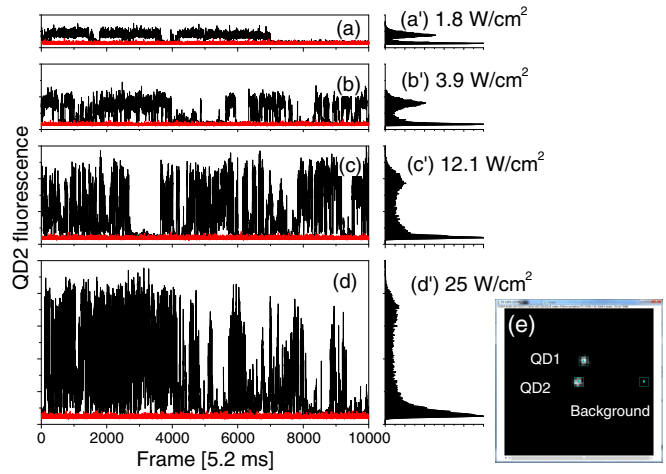

FIG. 1. (a)–(d) Four time series of fluorescence of a single water-soluble 3MPA-coated CdSe-CdS/CdZnS/ZnS QD [QD2 in (e)] under four different excitation powers (bin time = 5.2 ms). (a′)–(d′) Occurrence profiles of the on and off states. (e) One typical image frame under 12.1 W/cm^2 excitation showing the spatial locations of the QDs under study and the point where the background noise signal was extracted. The fluorescence time series of QD1 was qualitatively similar to that of QD2. The distance between QD1 and QD2 was ~1 μm, and the distance from the two QDs to the background point was ~3 μm. Note that the vertical scales of (a)–(d) and (a′)–(d′) are identical.

C. On/off probability density distributions

Figure 1 shows that the QD blinking feature was related to the excitation power. To quantify this relationship, we studied the effects of the excitation power on the on/off probability density distributions, which are presented in Figs. 2(a) and 2(b), showing clearly that the off-state probability density distribution obeyed the inverse power law and remained unchanged under different excitation powers. However, the on-state probability density distribution $\log_{10}[P_{on}(t)]$ became more linear with respect to t at high excitation power [excluding 12.1 and 25 W/cm^2, marked by the blue arrow, also because the output QD fluorescence per frame is not linear with respect to the excitation; see the reference lines in Fig. 2(b) and its inset].

Fluorescence blinking of all single QDs studied in this work and in Ref. [23] responded similarly to the excitation power variation. A similar dependence of the on- and off-state statistics on the excitation power was reported before [20]. Excluding the data for 12.1 and 25 W/cm^2 in Fig. 2(b) since the QD was flickering under these excitations, we observed a clear linear relationship between $\log_{10}[P_{on}(t)]$ and t under excitations of 1.8 and 3.9 W/cm^2.

A key factor to resolve temporal changes in a signal is the bin time (see, for example, Ref. [33]). Figures 2(c)–2(e) show the effects of the bin time on the on/off probability density distributions of one representative oil-soluble ODA-coated CdSe-CdS/CdZnS/ZnS QD under an excitation power

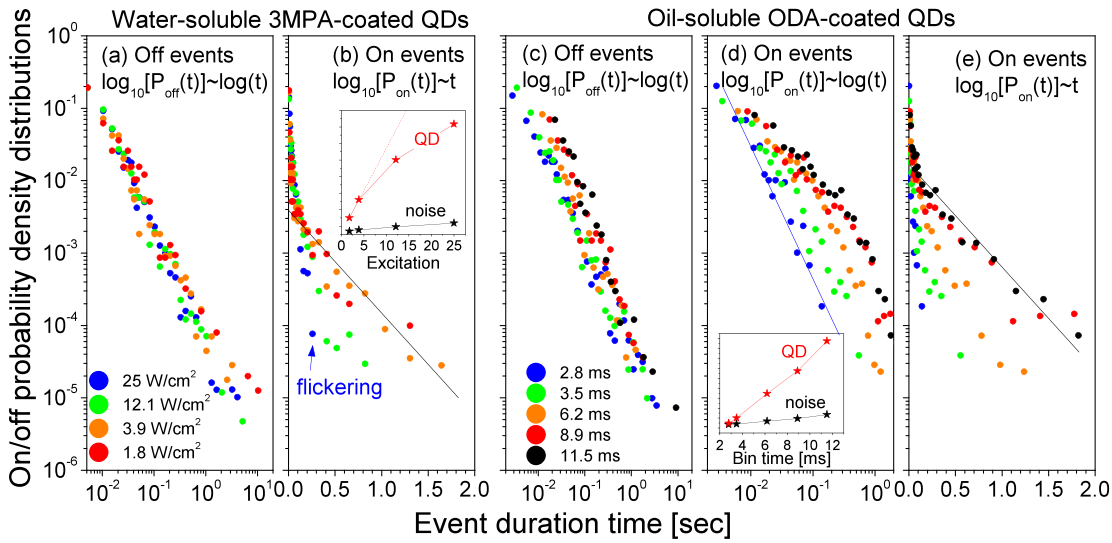

FIG. 2. (a) On-state and (b) off-state probability density distributions of the single 3MPA-coated CdSe-CdS/CdZnS/ZnS QD in Fig. 1 under four different excitation powers (bin time = 5.2 ms). (c)–(e) Dependence of on/off probability density distributions on bin time of a representative single ODA-QD (excitation power = 7.4 W/cm^2). Here $\log_{10}[P_{\rm off}(t)]$ remained largely linear with respect to $\log_{10}(t)$, and $\log_{10}[P_{\rm on}(t)]$ became linear with respect to t at long bin time. Insets in (b) and (d) are dependences of average QD fluorescence (red dots) and noise (black stars) per frame on excitation power and bin time.

of 7.4 W/cm^2. Here the excitation power was chosen such that $\log_{10}[P_{\rm on}(t)]$ was linear with respect to t. A very evident trend was observed here that the off-state probability density distribution remained unchanged; while $\log_{10}[P_{\rm on}(t)]$ was linear in $\log_{10}(t)$ at bin time of 2.8 ms, it approached linear in t (the random telegraph signal theory) at bin times of 8.9 and 11.5 ms [refer to the reference lines in Figs. 2(d) and 2(e)]. The bin time of 2.8 ms was too short, so the corresponding time series of the fluorescence was too noisy to be classified as blinking where the average QD fluorescence intensity per frame was almost the same as the noise [see inset in Fig. 2(d)]. Note also that the background noise signal was linearly proportional to the bin time [see inset in Fig. 2(d)], as it should be.

Figures 2(b) and 2(e) imply the necessity of a detailed assessment of the relationships between the measurement setup, microscopic physical processes, and the blinking characteristics.

III. THEORETICAL ANALYSIS

As mentioned before, high excitation power changed the characteristic appearance of QD fluorescence blinking. The modification in the on-state probability density distribution was attributed to multiexciton excitation, although multiexcitons were not observed directly [20]. The most likely reason why multiexcitons were not observed is the ultrafast speed of multiexciton dynamics. It was shown that biexciton lifetime, impact ionization, and Auger recombination rates in CdSe-based QDs were in the range of a few picoseconds [36,37]. Moreover, it is well known that a significant quantum efficiency of multiexciton generation in QDs was obtained only when the photon energy greatly exceeded the emission energy of the QDs [38], which was hardly the case in most QD fluorescence blinking measurements. In the current work, the excitation wavelength was 436 nm, and the QD fluorescence wavelengths were 601 and 622 nm, respectively.

A. Charge-tunneling surface-walking model

In reference to Fig. 3, we propose the following surface-state-associated CTSW model to understand the effects of the excitation power and the bin time reported in the previous section:

(1) Electron states in the QD core are characterized by two representative states: the excited state $E_{k'}$ and ground state E_k in the conduction band with quantum numbers k' and k and

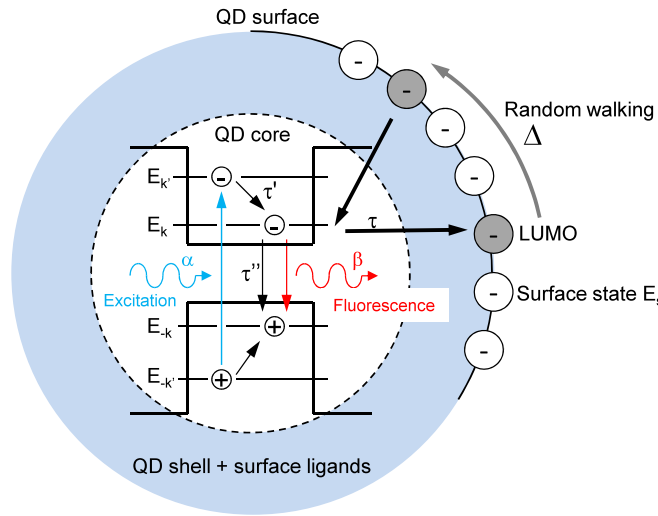

FIG. 3. Exciton transition paths in the surface-state-associated charge-tunneling surface-walking (CTSW) model. The two-dimensional surface random walk is schematically represented along the circle.

their occupations $n_{k'}$ and n_k by an electron; $E_{-k'}$ and E_{-k} are electron states in the valence band with occupations $n_{-k'}$ and n_{-k} by an electron.

(2) Optical excitation excites an electron originally occupying $E_{-k'}$ to $E_{k'}$ at a rate $1/\alpha$, leaving a hole at $E_{-k'}$.

(3) The electron relaxes from $E_{k'}$ to E_k, and the hole relaxes from $E_{-k'}$ to E_{-k} nonradiatively at rates $1/\tau'$.

(4) The electron at E_k and the hole at E_{-k} radiatively recombine at a rate $1/\beta$, resulting in the QD fluorescence.

(5) The electron at E_k and the hole at E_{-k} nonradiatively recombine at a rate $1/\tau''$. This nonradiative recombination was attributed to the observed redshift of emission from QDs immersed in immersion oil with a low thermal diffusivity compared with QDs in water [39]. Since major nonradiative energy relaxation processes in semiconductors have electron-phonon characteristics, we assume that $\tau'' = \tau'$. This gives a quantum efficiency of 60% when $\beta = 5$ ns and $\tau'' = 8$ ns, in agreement with the values of common CdSe-CdS/ZnS QDs [40].

(6) The photogenerated electron occupying E_k tunnels to the lowest unoccupied molecular orbital (LUMO) at the QD surface at a rate $1/\tau$. The LUMO is formed between semiconductor atoms of the QD and the 3MPA or ODA molecules on the QD surface [23,41]. In addition to the LUMOs on the QD surface, there are other surface states $\hbar\omega_s$ such as electron trap states [42]. LUMOs and $\hbar\omega_s$ are modeled to distribute randomly in a two-dimensional (2D) square grid on the QD surface. The electron, after tunneling from the QD core to one LUMO, randomly walks on the 2D grid until it reaches another nearby LUMO, parameterized by migration distance Δ. At this time point, the event of tunneling to the QD core is checked. A higher surface-state density implies a longer migration distance for the electron before it tunnels back into the QD core.

After photoexcitation, there is a possibility that the high-energy electron-hole pair can undergo impact ionization and Auger recombination processes. For the current blinking measurements of single QDs with emission wavelengths of 601 and 622 nm and an excitation wavelength of 436 nm, the rates of impact ionization and Auger recombination were negligible [37], so these two processes were not included in the numerical studies. Moreover, there is also the highest occupied molecular orbital that the photogenerated hole at E_{-k} may tunnel to and from. However, the tunneling of a hole in the valence band is, in general, very small due to the large effective mass of the hole, so it is not included in the model.

B. Heisenberg equations of motion

The CTSW model depicted in Fig. 3 was similar to the one published before [32] but extended to include nonradiative energy relaxation processes of a photoexcited electron and hole in the conduction and valence bands. Moreover, the rate equations presented in [32] were based on the Pauli exclusion principle that the occupation of one electron state reduces the efficiencies of transitions to this state since each state can be occupied by only one electron. To rigorously obtain the Heisenberg equations of motion of the electron-hole pair, we consider the following electron-hole pair system in a photon field:

$$H = E_k a_k^\dagger a_k + E_{-k} b_{-k}^\dagger b_{-k} + g^* a_k^\dagger b_{-k}^\dagger a + g b_{-k} a_k a^\dagger + \hbar\omega\left(a^\dagger a + \tfrac{1}{2}\right), \tag{1}$$

where $a_k^\dagger$ (creation of an electron at E_k) and a_k obey the anticommutation relations and so do $b_{-k}^\dagger$ (creation of a hole at E_{-k}) and b_{-k}. Here $a^\dagger$ is the creation of a photon, and $\hbar\omega$ is the photon energy; g describes the strength of the electron-photon interaction. The equation of motion of a physical parameter A is

$$\frac{dA}{dt} = \frac{i}{\hbar}[H, A] + \frac{\partial A}{\partial t}, \tag{2}$$

where $\partial A/\partial t$ is usually approximated as $\Lambda - \gamma A/\hbar$, where Λ describes the pump rate (such as electron injection in a laser operation) and $\hbar/\gamma$ describes the lifetime and broadening of the electron state [43]. Since we consider a closed electron system here, the pump rate is not included.

From the above equation, the temporal change of the electron state number operator $a_k^\dagger a_k$ is

$$\frac{\partial a_k^\dagger a_k}{\partial t} = \frac{i}{\hbar}[H,\ a_k^\dagger a_k]. \tag{3}$$

A careful study results in the following spontaneous radiative emission:

$$\left.\frac{\partial n_k}{\partial t}\right|_{\text{spont}} = -\frac{2\gamma|g|^2 n_k(1-n_{-k})}{\hbar[(E_k + E_{-k} - \hbar\omega)^2 + \gamma^2]}, \tag{4}$$

where $\langle a_k^\dagger a_k\rangle = n_k$ is the occupation of E_k by an electron and $\langle b_{-k}^\dagger b_{-k}\rangle = 1 - n_{-k}$ is the occupation of E_{-k} by a hole. It is easy to observe that

$$\frac{1}{\beta} = \frac{2\gamma|g|^2}{\hbar[(E_k + E_{-k} - \hbar\omega)^2 + \gamma^2]} \tag{5}$$

is the spontaneous radiative recombination rate of the electron-hole pair [44], which was experimentally measured and validated for our CdSe-CdS/ZnS core-multishell QD when we analyzed the time-resolved fluorescence decay spectrum measurement setup [45]. We obtain the Heisenberg equation of motion of n_k due to spontaneous radiative emission,

$$\frac{dn_k}{dt} = -\frac{n_k(1-n_{-k})}{\beta}, \tag{6}$$

which is the same as that obtained using the Pauli exclusion principle.

By including the photogeneration, nonradiative energy relaxations, tunneling, and random walks, the Heisenberg equations of motion of the electron in Fig. 3 are

$$\frac{dn_{k'}}{dt} = \frac{n_{-k'}(1-n_{k'})}{\alpha} - \frac{n_{k'}(1-n_k)}{\tau'},$$

$$\frac{dn_k}{dt} = \frac{n_{k'}(1-n_k)}{\tau'} - \frac{n_k(1-n_{-k})}{\tau''} - \frac{n_k(1-n_{-k})}{\beta} - \frac{n_k(1-n_s)}{\tau} + \frac{n_s^*(1-n_k)}{\tau},$$

$$\frac{dn_s}{dt} = \frac{n_k(1-n_s)}{\tau} - \frac{n_s(1-n_s^*)}{\eta}\cdots,$$

$$\frac{dn_s^*}{dt} = \frac{n_s(1-n_s^*)}{\eta} - \frac{n_s^*(1-n_k)}{\tau},$$
$$\frac{dn_{-k}}{dt} = \frac{n_{-k'}(1-n_k)}{\tau'} + \frac{n_k(1-n_{-k})}{\tau''} + \frac{n_k(1-n_{-k})}{\beta},$$
$$\frac{dn_{-k'}}{dt} = -\frac{n_{-k'}(1-n_{k'})}{\alpha} - \frac{n_{-k'}(1-n_{-k})}{\tau'}, \quad (7)$$

where $1/\eta$ is the random-walk rate between two neighboring surface states, $\hbar\omega_s$ and $\hbar\omega_s^*$.

We noticed some differences with the rate equations in the literature. For example, in the random telegraph signal model [15], the change in the probability of finding the QD at state i is proportional only to the probability of the other state(s) j that is coupled to state i. This is valid for low excitations such that state i is always initially unoccupied.

By deleting the charge-tunneling and surface-walking terms, the CTSW model in Eqs. (7) reduces to the time-dependent quantum model applied to studying multiphoton excitation of our QDs at a femtosecond timescale [46,47] and to studying the QD fluorescence lifetime on a nanosecond timescale [45]. Furthermore, autocorrelation analysis [15,26,27] of both the experimental and CTSW-model fluorescence time series was applied in order to assess the randomness of the on- and off-state events where a clear association was obtained between the observed linear relationship of $\log_{10}[P_{\rm on}(t)]$-t and a high degree of randomness at the millisecond timescale, partially affirming the CTSW model in that the on-state events are mostly random, while the off-state events are correlated via the series of random walks in the two-dimensional surface-state network [32].

C. Monte Carlo simulations

The CTSW model adopted the following temporal parameters: $\alpha = 10$ ps, $\tau' = \tau'' = 8$ ns, $\beta = 5$ ns, $\tau = 0.1$ s, all determined by quantum-mechanical calculations and independent experiments [32,45,48–50]. A similar τ was presented in the CTST model [31]. $\tau' = \tau'' = 8$ ns is much longer than many individual energy relaxation processes in nanometer CdSe and CdSe/ZnS heterostructures, such as the picosecond-order Auger-type energy relaxation process [37,51], and picosecond-order $1P$-to-$1S$ intraband electron relaxation obtained by measuring femtosecond transient absorption of CdSe QDs [52]. On the other hand, there have been extensive experimental works demonstrating long relaxation times on the order of nanoseconds in nanostructures (e.g., see Refs. [53,54]). Relaxation time longer than 1 ns was reported in colloidal CdSe QDs [55]. A major difference between the short and long energy relaxation processes is that the former involves limited numbers of discrete energy levels and energy relaxation processes, while the numbers of energy levels and energy relaxation processes in the latter are much higher. When multiple phonon effects were included in a perturbation calculation, a nanosecond-order electron energy relaxation was obtained [56]. We further notice the fact that the density of exciton states in the QD increases drastically when the exciton energy becomes higher than the energy of the ground exciton state (see, e.g., Ref. [37]), and it is clearly reflected in the absorption spectrum of the QD that the absorption of the QD increases very quickly when the photon energy exceeds the energy of the first absorption peak. $\tau' = \tau'' = 8$ ns was thus adopted here.

As mentioned before, our excitation intensity varied from 1.8 to 25.0 W/cm^2. It was estimated that the average time interval between two successive incident photons varied from 1289 to 92 ns [23]. The probability of multiple photons per 1 ns (the temporal resolution in the simulations; see below) is negligible. Multiphoton and multiexciton effects were thus not included in the simulations.

The Monte Carlo method was adopted to solve Eqs. (7) ranging from 1 ns to 1 s at a temporal step of 1 ns; 10 000 and 100 000 frames were simulated. All processes shown in Fig. 3 were continuously simulated, except the photon register, which was open for the first 4.29 ms and then closed for the following 0.91 ms to mimic the EMCCD camera action (exposure time of 4.29 ms and readout time of 0.91 ms; total time per frame was 5.2 ms). The total number of simulation loops for 10 000 frames was $10\,000 \times 5\,200\,000 = 5.2 \times 10^{10}$. This set the first constraint on the simulation since there is not a well-established random-number generator to generate a random-number series of arbitrary length. The second numerical constraint was set by the small tunneling probability. When the time step in the simulation was set to 1 ns so that we could resolve the discrete nature of the energy relaxation ($\tau' = \tau'' = 8$ ns) and radiative recombination ($\beta = 5$ ns) events, the tunneling probability was only 1 ns/$\tau = 10^{-8}$ per each time step, meaning that the random numbers needed a precision of 15–17 decimal digits for a numerically meaningful comparison between the random number and the tunneling probability. We used the best documented function routine RAN2 from [57]. Gaussian noise using the polar-rejection algorithm [58] was added, so that the noise spectrum thus obtained fitted the one of 3.9 W/cm^2 in Fig. 1 when assuming that 5% of the total emitted photons reached the photodetector (the emitted photon could assume any spatial propagation direction, while the photodetector covered only a tiny fraction of all possible directions).

In Monte Carlo simulations we set $\Delta = \text{rand} \times 9$, where rand is a random number, so that we could simulate variations in the surface state density. Figure 4 shows the fluorescence time series of different bin times (the ratio between exposure and readout was fixed to 4.29:0.91) excited by 25 and 3.9 W/cm^2. For the three bin times, the total time durations of the simulations were $0.52 \times 10\,000 = 5.2 \times 10^3$ ms $= 5.2 \times 10^9$ ns, 5.2×10^{10} ns, and 5.2×10^{11} ns. Since $\tau = 0.1$ s, we statistically expected ten tunneling events per 10^9 ns. For the three bin lengths, the statistically averaged numbers of tunneling events for 10 000 frames should be 50, 500, and 5000, while the numbers of tunneling events in Fig. 4 were $\sim$10 times less. We took a close look at the function routine RAN2 and noticed that the occurrence probability of random numbers smaller than 10^{-8} (which was the tunneling probability per 1 ns) was less than 10^{-9}, most likely due to the limited numerical precision. In the calculation of Fig. 5 we decreased τ from 0.1 to 0.01 s to tackle the problem. This, however, modified the off probability density distribution towards the random telegraph signal theory.

For the 25 W/cm^2 excitation, the statistical average number of incident excitation photons was 1 per 92 ns. In each

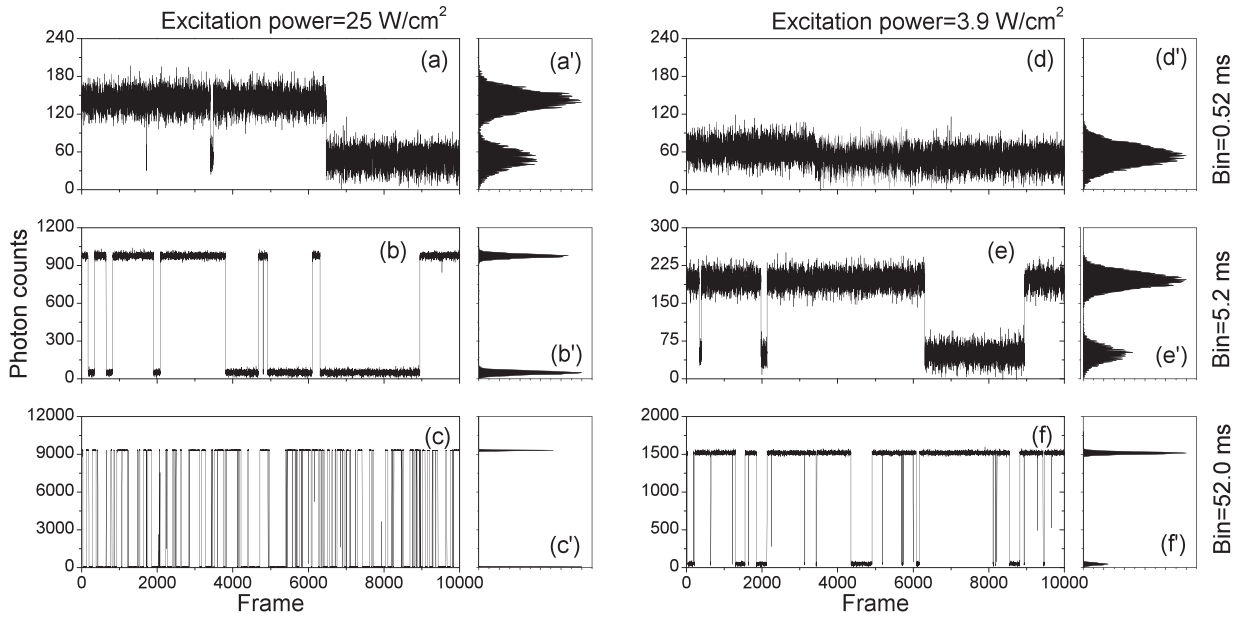

FIG. 4. (a)–(f) Time series of fluorescence under excitations of 25 and 3.9 W/cm^2 measured with different bin times. (a′)–(f′) Occurrence profiles of the on and off states. $\Delta = \text{rand} \times 9$, $\alpha = 10$ ps, $\tau' = \tau'' = 8$ ns, $\beta = 5$ ns, $\tau = 0.1$ s.

bin time of 0.52 ms (0.43 ms was the exposure time), we expected approximately $0.43 \times 10^6/92 \times 60\% = 2804$ emitted photons (in all directions, 60% is the quantum efficiency). Assuming that 5% of them reach the photodetector, ∼140 photons per frame are expected, which can be resolved in the temporal development of the photon emission using a bin window of 0.52 ms, as shown in Fig. 4(a). For 3.9 W/cm^2, there were only 22 photons per bin window, totally submerged by the noise [see Fig. 4(d)]. We thus had to increase the bin time to resolve the photon emission for 3.9 W/cm^2 [see Fig. 4(e)].

Next, we fixed the bin time to 5.2 ms and calculated the time series of fluorescence under different excitation powers for $\Delta = 0$ and $\Delta = \text{rand} \times 9$, and the numerical results are presented in Figs. 5(a) and 5(b). The evident disparity between the time series in Figs. 5(a) and 5(b) has a straightforward reason: the time duration of the off-state events are prolonged by the 2D random walk of the electron on the QD surface states.

For $\Delta = \text{rand} \times 9$, the on/off probability density distributions of the simulated single-QD fluorescence time series under excitations of 1.8, 3.9, and 7.8 W/cm^2 are presented in Figs. 5(c) and 5(d), which agree quantitatively well with Figs. 2(a) and 2(b). More specifically, the excitation power did not modify the off-state probability density distribution (note that $\log_{10}[P_{\text{off}}(t)]$ is not totally linear in $\log_{10}(t)$ in Fig. 5(c) since τ was numerically reduced to 0.01 s). The increase in the excitation power reduced the occurrence of low emissions due to nonincident or less incident photon excitations, so that the short-time-duration on-state events became better resolved, resulting in the increased probabilities of the short-time-duration on-state events and the decrease in the probabilities of the long-time-duration on-state events. This made the on-state probability density distribution $\log_{10}[P_{\text{on}}(t)]$ more linear with respect to t at high excitation power.

The dependence of the on-state probability density distribution on the bin time is shown in Fig. 5(e) while keeping the excitation power at 7.8 W/cm^2. Quantitative agreements between experimental data in Figs. 2(d) and 2(e) with CTSW results in Fig. 5(e) are readily concluded. The key observations here are as follows: (1) the noise will be dominant in the short-bin-time measurement; (2) the finite readout time in the recording camera could break up a long-time on-state event into two or three short-time events, both of them modifying the linear $\log_{10}[P_{\text{on}}(t)]$-$t$ relationship towards a linear $\log_{10}[P_{\text{on}}(t)]$-$\log_{10}(t)$ relationship. A long bin time is thus preferable, which may not be easy experimentally since the measurement setup may drift during the measurement. In the extreme case, a too long bin time may join two separate on events into one.

We further applied the CTSW model to quantitatively understand the experimental data showing that a clear linear relationship between $\log_{10}[P_{\text{on}}(t)]$ and t was revealed when the QD surface was passivated and/or modified by various means [15,17,20,22,25,31,32]. And the result was straightforward: the surface state density of a well-passivated QD surface is low, so Δ is small, resulting in the observed linear relationship between $\log_{10}[P_{\text{on}}(t)]$ and t. By using a model tunnel time $\tau \propto e^{-\theta\ell}$ [48], where $1/\theta$ is a characteristic length of the electron wave function and ℓ is the QD shell thickness, we could reproduce quantitatively, as can be expected, the suppressed blinking in the large, multishell, and composition-graded QDs reported in Refs. [59–61].

IV. SUMMARY

QD fluorescence blinking has been extensively studied, and many sophisticated models have been proposed. One major issue is that there has not been a good numerical match between theoretical simulations and experimental

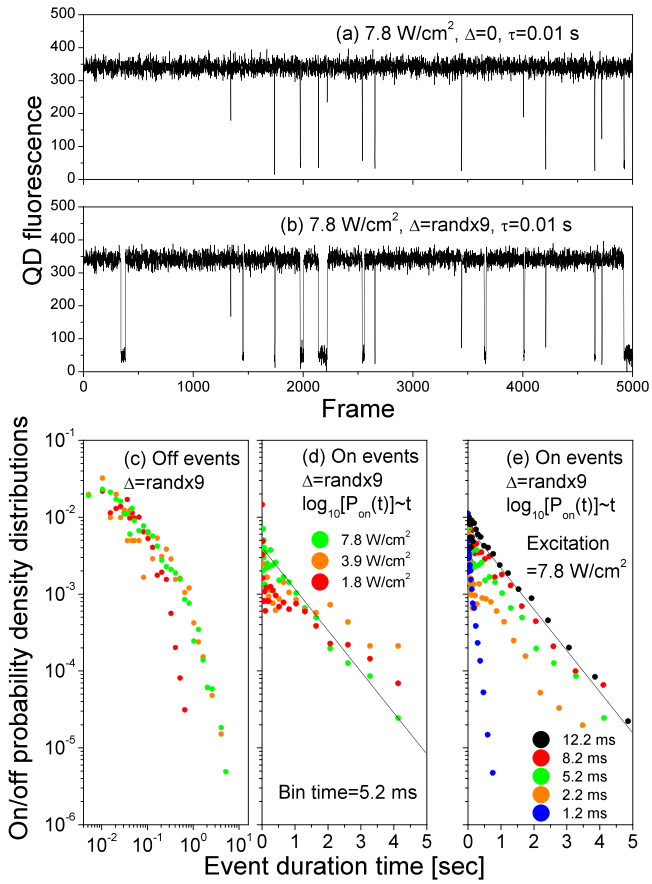

FIG. 5. (a) and (b) Time series of QD fluorescence under 7.8 W/cm^2 excitation, where $\Delta = 0$ and rand $\times$ 9, respectively. Here rand was a random number so that variations in the surface-state density could be simulated. (c) and (d) On/off probability density distributions of the single-QD fluorescence under excitations of 1.8, 3.9, and 7.8 W/cm^2 with bin time = 5.2 ms. (e) On-state probability density distributions of the single-QD fluorescence calculated using bin times from 1.2 to 12.2 ms (excitation power = 7.8 W/cm^2).

data. Another key aspect of QD fluorescence blinking is to study measurement setups necessary to resolve the underlying physical mechanisms of a single QD's fluorescence blinking.

In this study, guided by theoretical study and numerical modeling spanning from 1 ns to tens of seconds at a temporal resolution of 1 ns, a measurement design, namely, the excitation power and bin time, was proposed and applied to resolve the intrinsic characteristics of the fluorescence blinking of single colloidal CdSe-CdS/ZnS core-multishell QDs in which the off-state probability density distribution $\log_{10}[P_{\rm off}(t)]$ is linear with respect to $\log_{10}(t)$ due to the series of random walks in the two-dimensional surface-state network of the photoexcited electron after tunneling from the QD core to the QD surface. The on-state probability density distribution $\log_{10}[P_{\rm on}(t)]$ is linear with respect to t because of the random radiative recombination of the photoexcited electron-hole pair in the QD core.

Increasing the excitation power and/or the bin time will resolve the on-state fluorescence events, thus unraveling the intrinsic characteristics, i.e., that $\log_{10}[P_{\rm on}(t)]$ is linear with respect to t. However, a too high excitation power may cause a QD to flicker, and a too long bin time may also lead to problems. For our ODA- and 3MPA-coated CdSe-CdS/CdZnS/ZnS and CdSe-CdS/ZnS core-multishell QDs and Axio Observer D1 microscope, an excitation power of $\sim$7.8 W/cm^2 for a bin time longer than 5.2 ms was necessary to resolve the linear relationship between $\log_{10}[P_{\rm on}(t)]$ and t.

Nanoparticles have been extensively studied, and their application potential has been vastly expanding. The methods and results presented in this work open perspectives for the experimental identification of intrinsic QD fluorescence characteristics as well as for developing novel quantitative optical means to probe the microscopic milieu around QDs through the resolution and quantification of the QD fluorescence. Furthermore, the correct identification of QD blinking will be an advantage and even a necessity in superresolution fluorescence microscopy, e.g., stochastic optical reconstruction nanoscopy [62,63].

ACKNOWLEDGMENT

This work was partially supported by the Swedish Foundation for Strategic Research (Forskningsinstitutsdoktorand 2015).

[1] G. H. Carey, A. L. Abdelhady, Z. Ning, S. M. Thon, O. M. Bakr, and E. H. Sargent, Chem. Rev. **115**, 12732 (2015).
[2] C. R. Kagan, E. Lifshitz, E. H. Sargent, and D. V. Talapin, Science **353**, aac5523 (2016).
[3] X.-J. Shang, J.-F. He, M.-F. Li, F. Zhan, H.-Q. Ni, Z.-C. Niu, H. Pettersson, and Y. Fu, Appl. Phys. Lett. **99**, 113514 (2011).
[4] J. Lim, Y.-S. Park, and V. I. Klimov, Nat. Mater. **17**, 42 (2018).
[5] W. C. W. Chan and S. Nie, Science **281**, 2016 (1998).
[6] X. Michalet, F. F. Pinaud, L. A. Bentolila, J. M. Tsay, S. Doose, J. J. Li, G. Sundaresan, A. M. Wu, S. S. Gambhir, and S. Weiss, Science **307**, 538 (2005).
[7] U. Resch-Genger, M. Grabolle, S. Cavaliere-Jaricot, R. Nitschke, and T. Nann, Nat. Methods **5**, 763 (2008).
[8] M. Molnár, Y. Fu, P. Friberg, and Y. Chen, J. Nanobiotechnol. **8**, 2 (2010).
[9] Y. K. Tak, W. Y. Kim, M. J. Kim, E. Han, M. S. Han, J. J. Kim, W. Kim, J. E. Lee, and J. M. Song, Anal. Chim. Acta **721**, 85 (2012).
[10] F. M. de Melo, D. Grasseschi, B. B. N. S. Brandão, Y. Fu, and H. E. Toma, ACS Appl. Nano Mater. **1**, 2858 (2018).
[11] A. M. Alkilany, A. Shatanawi, T. Kurtz, R. B. Caldwell, and R. W. Caldwell, Small **8**, 1270 (2012).
[12] J. Duan, Y. Yu, Y. Li, Y. Yu, Y. Li, X. Zhou, P. Huang, and Z. Sun, PLoS One **8**, e62087 (2013).
[13] J. G. Hinman, J. R. Eller, W. Lin, J. Li, J. Li, and C. J. Murphy, J. Am. Chem. Soc. **139**, 9851 (2017).

[14] J. M. Fontana, H. Yin, Y. Chen, R. Florez, H. Brismar, and Y. Fu, Int. J. Nanomed. **12**, 8615 (2017).

[15] Al. L. Efros and M. Rosen, Phys. Rev. Lett. **78**, 1110 (1997).

[16] M. Kuno, D. P. Fromm, H. F. Hamann, A. Gallagher, and D. J. Nesbitt, J. Chem. Phys. **112**, 3117 (2000); **115**, 1028 (2001).

[17] S. Hohng and T. Ha, J. Am. Chem. Soc. **126**, 1324 (2004).

[18] C. D. Heyes, A. Y. Kobitski, V. V. Breus, and G. U. Nienhaus, Phys. Rev. B **75**, 125431 (2007).

[19] P. Frantsuzov, M. Kuno, B. Jankó, and R. A. Marcus, Nat. Phys. **4**, 519 (2008).

[20] J. J. Peterson and D. J. Nesbitt, Nano Lett. **9**, 338 (2009).

[21] F. Stefani, J. Hoogenboom, and E. Barkai, Phys. Today **62**(2), 34 (2009).

[22] H. C. Ko, C. T. Yuan, S. H. Lin, and J. Tang, Appl. Phys. Lett. **96**, 012104 (2010).

[23] L. Li, G. Tian, Y. Luo, H. Brismar, and Y. Fu, J. Phys. Chem. C **117**, 4844 (2013).

[24] N. Amecke, A. Heber, and F. Cichos, J. Chem. Phys. **140**, 114306 (2014).

[25] Z. Gan, X. Wu, H. Xu, N. Zhang, S. Nie, and Y. Fu, J. Phys. D **49**, 275107 (2016).

[26] X. Brokmann, J.-P. Hermier, G. Messin, P. Desbiolles, J.-P. Bouchaud, and M. Dahan, Phys. Rev. Lett. **90**, 120601 (2003).

[27] G. Margolin and E. Barkai, Phys. Rev. Lett. **94**, 080601 (2005).

[28] J. Tang and R. A. Marcus, Phys. Rev. Lett. **95**, 107401 (2005).

[29] P. A. Frantsuzov, S. Volkán-Kacsó, and B. Jankó, Nano Lett. **13**, 402 (2013).

[30] R. Schmidt, C. Krasselt, C. Göhler, and C. von Borczyskowski, ACS Nano **8**, 3506 (2014).

[31] M. A. Osborne and A. A. Fisher, Nanoscale **8**, 9272 (2016).

[32] H. Xu, H. Brismar, and Y. Fu, J. Colloid Interface Sci. **505**, 528 (2017).

[33] C. H. Crouch, O. Sauter, X. Wu, R. Purcell, C. Querner, M. Drndic, and M. Pelton, Nano Lett. **10**, 1692 (2010).

[34] Z. Ning, H. Tian, H. Qin, Q. Zhang, H. Ågren, L. Sun, and Y. Fu, J. Phys. Chem. C **114**, 15184 (2010).

[35] Z. Ning, M. Molnár, Y. Chen, P. Friberg, L. Gan, H. Ågren, and Y. Fu, Phys. Chem. Chem. Phys. **13**, 5848 (2011).

[36] G. Bacher, R. Weigand, J. Seufert, V. D. Kulakovskii, N. A. Gippius, A. Forchel, K. Leonardi, and D. Hommel, Phys. Rev. Lett. **83**, 4417 (1999).

[37] Y. Fu, Y.-H. Zhou, H. Su, F. Y. C. Boey, and H. Ågren, J. Phys. Chem. C **114**, 3743 (2010).

[38] M. T. Trinh, A. J. Houtepen, J. M. Schins, T. Hanrath, J. Piris, W. Knulst, A. P. L. M. Goossens, and L. D. A. Siebbeles, Nano Lett. **8**, 1713 (2008).

[39] H. Xu, L. Li, O. Manneberg, A. Russom, K. B. Gylfason, H. Brismar, and Y. Fu, J. Phys. Chem. B **117**, 14151 (2013).

[40] W. Xu, X. Hou, Y. Meng, R. Meng, Z. Wang, H. Qin, X. Peng, and X. W. Chen, Nano Lett. **17**, 7487 (2017).

[41] K. E. Knowles, M. T. Frederick, D. B. Tice, A. J. Morris-Cohen, and E. A. Weiss, J. Phys. Chem. Lett. **3**, 18 (2012).

[42] C. Pu and X. Peng, J. Am. Chem. Soc. **138**, 8134 (2016).

[43] W. W. Chow, S. W. Koch, and M. Sargent III, *Semiconductor-Laser Physics* (Springer, Berlin, 1994) pp. 72, 333.

[44] L. D. Landau and E. M. Lifshitz, *Quantum Mechanics*, 2nd ed. (Pergamon, Oxford, 1965).

[45] H. Xu, V. Chmyrov, J. Widengren, H. Brismar, and Y. Fu, Phys. Chem. Chem. Phys. **17**, 27588 (2015).

[46] T.-T. Han, Y. Fu, and H. Ågren, J. Appl. Phys. **101**, 063712 (2007).

[47] Y. Fu, T.-T. Han, H. Ågren, L. Lin, P. Chen, Y. Liu, G.-Q. Tang, J. Wu, Y. Yue, and N. Dai, Appl. Phys. Lett. **90**, 173102 (2007).

[48] Y. Fu, O. Engström, and Y. Luo, J. Appl. Phys. **96**, 6477 (2004).

[49] Y. Fu, H. Ågren, J. M. Kowalewski, H. Brismar, J. Wu, Y. Yue, N. Dai, and L. Thylén, Europhys. Lett. **86**, 37003 (2009).

[50] M. A. Salem, H. Mizuta, S. Oda, Y. Fu, and M. Willander, Jpn. J. Appl. Phys. **44**, L88 (2005).

[51] Al. L. Efros, V. A. Kharchenko, and M. Rosen, Solid State Commun. **93**, 281 (1995).

[52] V. I. Klimov, D. W. McBranch, C. A. Leatherdale, and M. G. Bawendi, Phys. Rev. B **60**, 13740 (1999).

[53] K. Mukai, N. Ohtsuka, H. Shoji, and M. Sugawara, Appl. Phys. Lett. **68**, 3013 (1996).

[54] A. J. Nozik, Annu. Rev. Phys. Chem. **52**, 193 (2001).

[55] A. Pandey and P. Guyot-Sionnest, Science **322**, 929 (2008).

[56] T. Inoshita and H. Sakaki, Phys. B (Amsterdam) **227**, 373 (1996).

[57] S. A. Teukolsky, W. T. Vetterling, and B. P. Flannery, in *Numerical Recipes in FORTRAN: The Art of Scientific Computing*, 2nd ed., edited by W. H. Press (Cambridge University Press, Cambridge, 1992), Vol. 1, p. 266.

[58] P. H. W. Leong and J. D. Villasenor, ACM Comput. Surv. **39**, 11 (2007).

[59] Y. Chen, J. Vela, H. Htoon, J. L. Casson, D. J. Werder, D. A. Bussian, V. I. Klimov, and J. A. Hollingsworth, J. Am. Chem. Soc. **130**, 5026 (2008).

[60] J. Vela, H. Htoon, Y. Chen, Y. S. Park, Y. Ghosh, P. M. Goodwin, J. H. Werner, N. P. Wells, J. L. Casson, and J. A. Hollingsworth, J. Biophotonics **3**, 706 (2010).

[61] I. Hadar, J. P. Philbin, Y. E. Panfil, S. Neyshtadt, I. Lieberman, H. Eshet, S. Lazar, E. Rabani, and U. Banin, Nano Lett. **17**, 2524 (2017).

[62] M. Dahan, T. Laurence, F. Pinaud, D. S. Chemla, A. P. Alivisatos, M. Sauer, and S. Weiss, Opt. Lett. **26**, 825 (2001).

[63] P. Hoyer, T. Staudt, J. Engelhardt, and S. W. Hell, Nano Lett. **11**, 245 (2011).